JHEP|Reports

PPP1R15A-expressing monocytic MDSCs promote immunosuppressive liver microenvironment in fibrosis-associated hepatocellular carcinoma

Authors

Xiaoyu Liu, Man Liu, Haoran Wu, …, Stephen Lam Chan, Jingying Zhou, Alfred Sze-Lok Cheng

Correspondence

zhoujy@cuhk.edu.hk (J. Zhou), alfredcheng@cuhk.edu.hk (A. Sze-Lok Cheng).

Graphical abstract

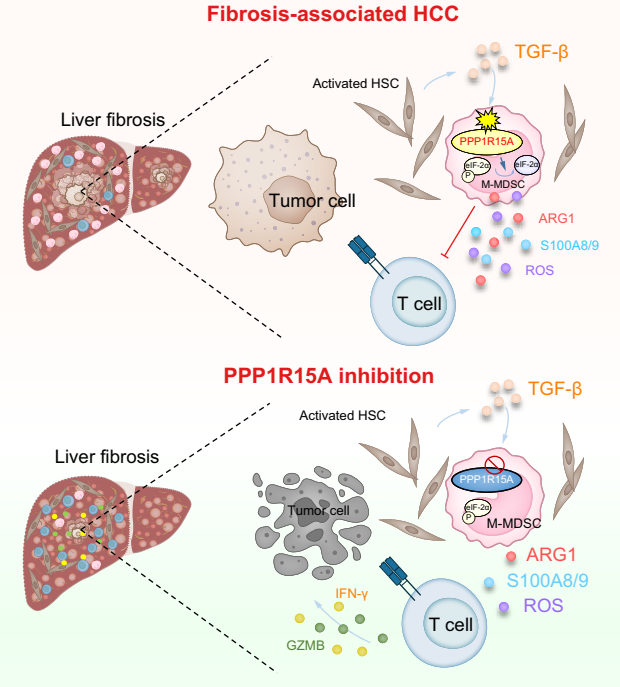

Highlights:

- PPP1R15A is selectively upregulated in M-MDSCs in patients with fibrosis-associated HCC.
- Knockdown of PPP1R15A suppresses M-MDSC functionality to restrict HCC growth and enhance ICB efficacy.
- Suppression of PPP1R15A reduces the immunosuppressive potential of fibrotic HCC patient-derived M-MDSCs.
- A *PPP1R15A*$^{+}$ M-MDSC signature correlates with poor prognosis and immunotherapy unresponsiveness in patients with cancer.

Impact and implications:

Our cross-species analysis has identified PPP1R15A as a therapeutic target governing the anti-T-cell activities of fibrosis-associated M-MDSCs (monocytic myeloid-derived suppressor cells). The results from the preclinical models show that specific inhibition of PPP1R15A can break the immunosuppressive barrier to restrict hepatocellular carcinoma growth and enhance the efficacy of immune checkpoint blockade. PPP1R15A may also function as a prognostic and/or predictive biomarker in patients with hepatocellular carcinoma.

https://doi.org/10.1016/j.jhepr.2024.101087

JHEP|Reports

PPP1R15A-expressing monocytic MDSCs promote immunosuppressive liver microenvironment in fibrosis-associated hepatocellular carcinoma

Xiaoyu Liu[1,2], Man Liu[3], Haoran Wu[1], Wenshu Tang[1], Weiqin Yang[1], Thomas T.H. Chan[1], Lingyun Zhang[1], Shufen Chen[1], Zhewen Xiong[1], Jianxin Liang[1], Willis Wai-Yiu Si-Tou[1], Ting Shu[1], Jingqing Li[1], Jianquan Cao[1], Chengpeng Zhong[4], Hanyong Sun[4], Tsz Tung Kwong[5], Howard H.W. Leung[6], John Wong[7], Paul Bo-San Lai[7], Ka-Fai To[6,8], Tingxiu Xiang[2], Joseph Jao-Yiu Sung[9,10], Stephen Lam Chan[5,8], Jingying Zhou[1,*], Alfred Sze-Lok Cheng[1,*]

JHEP Reports **2024**. vol. 6 | 1–14

Background & Aims: Recent studies demonstrated the importance of fibrosis in promoting an immunosuppressive liver microenvironment and thereby aggressive hepatocellular carcinoma (HCC) growth and resistance to immune checkpoint blockade (ICB), particularly via monocyte-to-monocytic myeloid-derived suppressor cell (M-MDSC) differentiation triggered by hepatic stellate cells (HSCs). We thus aimed to identify druggable targets in these immunosuppressive myeloid cells for HCC therapy.

Methods: M-MDSC signature genes were identified by integrated transcriptomic analysis of a human HSC-monocyte culture system and tumor-surrounding fibrotic livers of patients with HCC. Mechanistic and functional studies were conducted using *in vitro*-generated and patient-derived M-MDSCs. The therapeutic efficacy of a M-MDSC targeting approach was determined in fibrosis-associated HCC mouse models.

Results: We uncovered over-expression of protein phosphatase 1 regulatory subunit 15A (*PPP1R15A*), a myeloid cell-enriched endoplasmic reticulum stress modulator, in human M-MDSCs that correlated with poor prognosis and ICB non-responsiveness in patients with HCC. Blocking TGF-β signaling reduced PPP1R15A expression in HSC-induced M-MDSCs, whereas treatment of monocytes by TGF-β upregulated PPP1R15A, which in turn promoted ARG1 and S100A8/9 expression in M-MDSCs and reduced T-cell proliferation. Consistently, lentiviral-mediated knockdown of *Ppp1r15a in vivo* significantly reduced $ARG1^{+}S100A8/9^{+}$ M-MDSCs in fibrotic liver, leading to elevated intratumoral IFN-$\gamma^{+}GZMB^{+}CD8^{+}$ T cells and enhanced anti-tumor efficacy of ICB. Notably, pharmacological inhibition of PPP1R15A by Sephin1 reduced the immunosuppressive potential but increased the maturation status of fibrotic HCC patient-derived M-MDSCs.

Conclusions: $PPP1R15A^{+}$ M-MDSC cells are involved in immunosuppression in HCC development and represent a novel potential target for therapies.

Introduction

Hepatocellular carcinoma (HCC) represents the most common primary liver cancer and the second most common cause of cancer-related death worldwide.[1] Approximately 70-90% of patients with HCC have concurrent liver fibrosis or cirrhosis which are associated with risk factors including viral hepatitis infection and non-alcoholic fatty liver disease.[1] Treatment of HCC remains challenging, due to its heterogeneity, lack of early diagnostic biomarkers, tumor-escape mechanisms, frequent relapse upon surgery, and marginal effect of the available molecular therapies. Immunotherapies that inhibit immune-checkpoints such as cytotoxic T-lymphocyte associated protein 4, programmed cell death 1 or its ligand 1 (PD-L1), result in remarkably durable anti-tumor T-cell responses in around 20% of patients with advanced HCC.[2] Nevertheless, the relatively low response rates in HCC compared to other 'hot' cancers like non-small cell lung cancer (NSCLC) and melanoma emphasize the strong immunosuppressive barrier that urgently needs remediation. Interestingly, these ICB antibodies achieved better response rates in patients with HCC co-treated with sorafenib or the VEGF (vascular endothelial growth factor) inhibitor bevacizumab, which may be due to its immunomodulatory effects on reducing immunosuppressive cells, especially myeloid-derived suppressor cells (MDSCs) in the tumor microenvironment (TME).[3–6]

MDSCs are a heterogeneous group of immature myeloid cells characterized by their potent ability to suppress anti-tumor T-cell responses.[7] Two major subsets of MDSCs have been identified: monocytic (M-MDSC) and polymorphonuclear

* Corresponding authors. Address: Lo Kwee-Seong Integrated Biomedical Sciences Building, Area 39, The Chinese University of Hong Kong, Shatin, Hong Kong, China.
E-mail addresses: zhoujy@cuhk.edu.hk (J. Zhou), alfredcheng@cuhk.edu.hk (A. Sze-Lok Cheng).
https://doi.org/10.1016/j.jhepr.2024.101087

(PMN-MDSC), which share phenotypic and morphologic features with monocytes and neutrophils, respectively.[7] The heterogeneity of phenotypic and functional features of MDSCs among and within different cancer types highlights the importance of MDSC subset characterization in specific tumor contexts. Of note, our previous findings have pinpointed that PMN-MDSCs are mainly accumulated in the TME, while M-MDSCs are preferably enriched in peritumoral fibrotic livers induced by pro-fibrogenic hepatic stellate cells (HSCs) in HCC.[8–11] Targeting the HSC-M-MDSC crosstalk could therefore release M-MDSC-mediated immunosuppression to restrict tumor growth in fibrotic livers and enhance ICB responsiveness in fibrosis-associated HCC mouse models.[10] Clinically, this M-MDSC subset abundance is associated with poor prognosis in patients with HCC.[10] Besides, a high level of circulating M-MDSCs is reported to be correlated with ICB resistance in patients with advanced NSCLC or melanoma.[12,13] Despite this substantial progress, key knowledge gaps in identifying M-MDSC signature genes for specific M-MDSC targeting in HCC remain to be addressed. Here, we employed integrated analysis of single-cell RNA-sequencing (scRNA-seq) in tumor-surrounding fibrotic liver tissues of patients with HCC and bulk RNA-seq of HSC-induced M-MDSCs to identify M-MDSC signature genes for HCC therapy.

Materials and methods

Materials

Cell lines: RIL-175 (a generous gift from Prof. Lars Zender and Prof. Tim Greten) and LX2 cells purchased from Merck Millipore (#SCC064) were used. All cell lines were cultured in DMEM (Gibco), supplemented with 10% FBS (Gibco) in a 37 °C humidified chamber with 5% CO_2.

Human specimens: Paired tumor and adjacent liver tissues from patients with HCC were collected for immunohistochemical analyses. Single cells isolated from whole blood, tumor, and adjacent liver tissues from patients with HCC were collected for flow cytometry and drug treatment. All HCC patient specimens were from those who underwent liver resection at the Prince of Wales Hospital (Hong Kong). Buffy coats from healthy subjects collected from Hong Kong Red Cross were used for *in vitro* generation of M-MDSCs. Parental/guardian consent was obtained. Studies using human specimens were approved by the joint CUHK-NTEC Clinical Research Ethics.

Mice: All animal experiments were approved by the Animal Experimentation Ethics Committee of the Chinese University of Hong Kong (AEEC-CUHK). C57BL/6 male mice were maintained according to standard operating procedures at CUHK Laboratory Animal Services Centre.

Methods

Integrated analysis of bulk RNA-seq and scRNA-seq datasets

Differentially expressed genes (DEGs) from *in vitro*-generated M-MDSCs compared with monocytes were determined from our previous dataset.[10] HCC scRNA-seq processed data of myeloid cells were downloaded[14] and processed using Seurat 4.3.0. M-MDSC were annotated as $CD14^+$ myeloid cells. DEGs were identified using the Wilcoxon rank sum test.

Primary cell isolation and flow cytometry analysis

Peripheral blood mononuclear cells (PBMCs) were freshly isolated from buffy coats of anonymous human healthy donors using Ficoll-Paque Premium (GE Healthcare). Single cells were isolated from fresh liver and tumor tissues by chopping and digested in collagenase D and DNase I (Invitrogen). Cells were collected then incubated with Fcγ blocking antibody for 15 min at 4 °C and stained with surface markers. The human M-MDSC is defined by $CD45^+CD11b^+CD33^+CD14^+HLA\text{-}DR^{-/low}$, while mouse M-MDSC is defined by $CD45^+CD11b^+Gr\text{-}1^+Ly\text{-}6C^+Ly6G^-$. The macrophages are differentiated from M-MDSC with $CD45^+CD11b^+CD33^-F4/80^+$ (human) and $CD45^+CD11b^+Gr\text{-}1^-F4/80^+$ (mouse). The monocytes are also differentiated from M-MDSC with $CD45^+CD11b^+CD14^+HLA\text{-}DR^+$ (human) and $CD45^+CD11b^+Gr\text{-}1^-F4/80^-CD11c^-Ly\text{-}6C^+$ (mouse). Subsequently, cells were permeabilized and stained with intracellular markers according to the manufacture's instruction (BD Biosciences). Flow cytometry data were acquired by BD FACSymphony A5.2 or FACSAria Fusion (BD Biosciences) and analyzed by FlowJo software (Tree Star). The flow antibodies used in this study were listed in Table S1.

Co-immunofluorescence staining

Tissues from patients or mice were collected and fixed in 4% paraformaldehyde (Sigma-Aldrich) for 24 h, washed in 70% ethanol, and embedded in paraffin. Five-millimeter sections from paraffin-embedded tissues were deparaffinized, rehydrated, and rinsed in distilled water. Immunofluorescence staining was performed manually using the Opal 7-Color IHC Kits (PerkinElmer) according to the manufacturer's protocol against human CD8, CD14, CD33 and PPP1R15A. Nikon Ti2-E Inverted Fluorescence Microscope was applied for the image acquisition. The antibodies used in this study were listed in Table S1.

Quantitative real-time PCR

RNA was extracted by RNA extraction kit (Shanghai Fastagen Biotechnology, cat#: 220010) and incubated PrimeScript RT Master Mix (Takara) for cDNA synthesis according to the manufacturer's instruction. Power SYBR Green PCR Master Mix (Takara) and QS7 Real-Time PCR System (Applied Biosystems) were utilized for cDNA application and expression quantification. The primers used for this study were listed in Table S2.

Western blot

Protein was extracted in protein lysis buffer supplemented with protease inhibitor and phosphatase inhibitor cocktail (Bimake), followed by 8-12% SDS-PAGE (Bio-Rad). The immunoblotting signals were detected with a Chemiluminescence kit (WesternBright ECL; or WesternBright Sirius) and ChemDoc Imaging System (Bio-Rad). Western blot antibodies used in this study were listed in Table S1.

M-MDSC generation and functionality analysis

Monocytes isolated from healthy donor PBMCs by human CD14 microbeads were cultured in LX2 conditioned medium

(LX2-CM) at 2*10^6 cell/ml density for M-MDSC induction, or in normal medium (DMEM supplemented with 10% FBS) as control. Gene modulation and drug treatment were conducted in LX2-CM-induced M-MDSCs followed by phenotypic and functional analysis. The sequences of human short-hairpin RNA (shRNA) were listed in Table S3. Reactive oxygen species (ROS) was detected by measuring CM-H2DCFDA. For T-cell suppression assay, $CD3^+$ cells were purified by human CD3 microbeads and labeled with CFSE (5 μmol/L; Invitrogen), and then co-cultured with M-MDSCs (1:1) in the presence of CD3/CD28 dynabeads (Invitrogen) and human recombinant IL-2 (R&D) for 4 days. T cells with or without dynabeads stimulation were used as the positive or negative control, respectively. Surface staining for CD3 and CFSE signals on T cells were acquired by flow cytometry using FACSAria Fusion (BD Biosciences). The percentages of proliferating cells were determined and calculated by FlowJo software (Tree Star).

Fibrosis-associated HCC mouse models

Orthotopic HCC mouse models. The High-fat-high-carbohydrate (HFHC) HCC mouse model was established as previously reported.[15,16] Briefly, 4-6-week-old C57BL/6 mice were fed with HFHC diet plus drinking water enriched with high-fructose corn syrup for 16 weeks, followed by intrahepatic injection of 1x10^6 RIL-175 cells. The lentivirus-mediated shRNA was prepared as previously described,[17] and injected into mice by tail vein (5x10^7 TU/mouse) 5 days before tumor inoculation.

The carbon tetrachloride (CCl_4)-induced HCC mouse model was established by administering 5-6-week-old C57BL/6 male mice with CCl_4 via gavage for 8 weeks, followed by intrahepatic injection of 5x10^5 RIL-175 cells.[15,16] Lentivirus-mediated shRNA was injected to the mice 5 days before tumor implantation. Mice were then subjected to IgG or anti-PD-L1 treatment via intraperitoneal injection (10 mg/kg) on day 5, 11 and 16 after tumor inoculation as described previously.[8,10,11]

All mice were sacrificed at 3 weeks post-tumor cell implantation or humane endpoint. The sequences of mouse shRNA were listed in Table S3.

Spontaneous HCC mouse model. 2-day-old C57BL/6 male mice were intraperitoneally injected with a single dose of streptozocin (STZ) and fed with HFHC diet from the age of 4 to 19 weeks.[15,16] The mice were euthanized at week 19 and the tumor burden was measured. Tumor and matched non-tumor liver tissues were collected for flow cytometry and PCR analyses.

Online patient dataset analysis

mRNA levels and survival data of liver hepatocellular carcinoma (LIHC) from The Cancer Genome Atlas (TCGA) was obtained from the University of California, Santa Cruz (UCSC; http://xena.ucsc.edu/). LIHC samples were stratified into high (30%) and low (30%) groups according to the mRNA level of *PPP1R15A, CD14, ARG1, S100A8,* and *S100A9*. Patients in the high or low group were then compared for their overall survival and plotted in standard Kaplan-Meier curves. To explore the potential role of *PPP1R15A* on immunotherapy responsiveness, TIDE (tumor immune dysfunction and exclusion) scores were calculated by the TIDE algorithm (http://tide.dfci.harvard.edu/), according to the developer's instructions. The cut-off value of 0 in the TIDE score was used to predict the immunotherapy response of each tumor sample. To study the correlation between *PPP1R15A*$^+$ M-MDSC and survival in immunotherapy-treated patients, patients were classified into high and low groups based on the medium cut-off. Overall survival analysis was then visualized by Kaplan-Meier plots using publicly available cancer patient datasets.

Statistical analysis

Data were analyzed using GraphPad Prism 8 and are presented as mean ± SEM. Statistical comparison between two groups was evaluated by two-tailed and unpaired Student's *t* test. Paired Student's *t* test was used to compare pre-treatment and on-treatment samples. Non-parametric test was used when data does not adhere to normal distribution. One-way ANNOVA was used for the comparison among multiple groups. Two-way ANOVA was applied for the comparison among multiple groups on a continuous variable. Correlation analysis was performed using single-tailed Pearson correlation. Kaplan-Meier survival analysis was performed by log-rank (Mantel-Cox) test. The relationship between two categorical variables was computed by the Chi-square test. A *p* value smaller than 0.05 was considered statistically significant.

Results

Transcriptomic analysis identifies *PPP1R15A* as a novel signature gene in M-MDSCs from patients with HCC with liver fibrosis

We have previously established a M-MDSC *in vitro* generation assay by culturing human $CD14^+$ cells with CM from an activated human HSC cell line LX2, which recapitulates major features of hepatic M-MDSCs from fibrosis-associated patients with HCC.[10] Compared to untreated $CD14^+$ cells, bulk RNA-seq analysis has uncovered 564 DEGs (p <0.05, log2 fold-change >1) in these M-MDSCs (Fig. 1A).[10] In parallel, we re-analyzed the scRNA-seq data from patients with HCC[14] with enrichment of the myeloid cell barcodes by Seurat 4.3.0 and identified 499 DEGs (p <0.05) enriched in $CD14^+$ M-MDSC-like cell clusters compared to the resting myeloid cell clusters, in which 65 DEGs were overlapped with those derived from the LX2-CM-induced M-MDSCs (Table S4). These DEGs contained well-studied MDSC signature genes that have been reported to play critical roles in MDSC trafficking and immunosuppression including *CCL2*, *CCL20*, *CXCL2*, *CXCL3*, *IL-1b*, and *ARG1*, *S100A8*, *S100A12*,[7] thus validating the authenticity of our transcriptomic analysis.

Therefore, we further conducted the analysis on the correlations of these 65 DEGs towards the well-known M-MDSC marker genes (*CD14, ARG1, S100A8, S100A9*) in tumor-adjacent livers from patients with HCC in TCGA (n = 48) and liver tissues from GETx cohort (n = 110) as well as their expression profiling in 79 human tissues and cells (GeneAtlas U133A dataset). Interestingly, we have identified a novel M-MDSC target gene, *i.e.* protein phosphatase 1 regulatory subunit 15A (*PPP1R15A*), which was not only positively correlated with the M-MDSC signature (Fig. 1B), but also showed a specific enrichment in $CD33^+$ myeloid cells compared to other tissues or cells (Fig. 1C). The upregulation of *PPP1R15A* mRNA and protein levels were also verified in LX2-CM-induced M-MDSCs compared to naïve monocytes

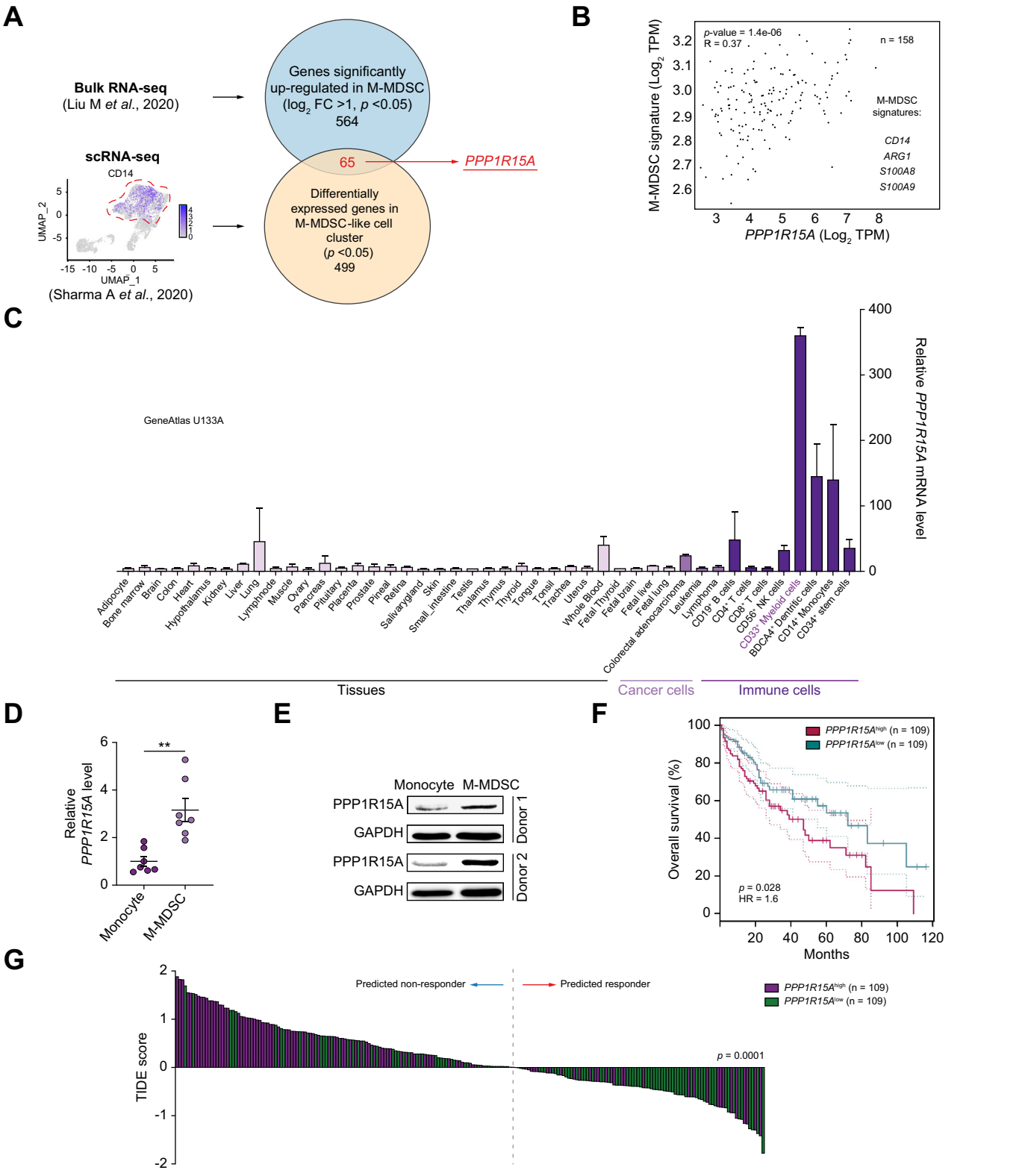

Fig. 1. Transcriptomic analysis identifies *PPP1R15A* as a novel signature gene in M-MDSCs from patients with HCC with liver fibrosis. (A) Venn diagram of DEGs in $CD45^+CD11b^+CD33^+CD14^+HLA\text{-}DR^{-/low}$ M-MDSCs identified by *in vitro*-generated and HCC patient-derived M-MDSCs. 564 DEGs were identified by bulk RNA-seq when comparing *in vitro*-generated M-MDSCs to monocyte controls[10] (Wald-test). 499 DEGs were identified in M-MDSC-like cell cluster ($CD14^+$) compared to the rest of myeloid cell clusters from qualified myeloid cell barcodes by reanalysis of a scRNA-seq dataset from HCC patient tissues[14] (Wilcoxon rank sum test). (B) The mRNA level (RSEM) of *PPP1R15A* positively correlated with M-MDSC marker genes (*CD14, ARG1, S100A8, S100A9*) in tumor-adjacent livers from patients with HCC in TCGA database (n = 48) and liver tissues from GETx cohort (n = 110) (generated by GEPIA2). (C) *PPP1R15A* mRNA level from GeneAltlas U133A dataset (generated by biogps) in indicated tissues, cancer cells and immune cells. (D) M-MDSCs were generated by culturing $CD14^+$ monocytes with LX2-CM for 7 days. The mRNA (p = 0.0016, paired t test. Data were presented as mean±SE; **, p <0.01) and (E) protein levels of PPP1R15A in *in vitro* M-MDSCs and monocytes were

(Fig. 1D,E). Moreover, high *PPP1R15A* expression correlated with poor overall survival of patients with HCC (hazard ratio = 1.6, p <0.05; Fig. 1F). Using the TIDE analysis, which integrates the expression signatures of T-cell dysfunction and T-cell exclusion to predict ICB response,[18] and the HCC TCGA dataset, we found that patients with HCC and high expression of *PPP1R15A* were significantly more susceptible to ICB resistance than those with HCC and low *PPP1R15A* expression (p <0.001; Fig. 1G). PPP1R15A, also known as growth arrest and DNA damage-inducible protein 34 (GADD34), is an important modulator of endoplasmic reticulum stress that controls ROS induction.[19] Notably, *Ppp1r15a* knockout mice exhibited a significant reduction in tumor incidence in carcinogen-induced tumor models of both the colon and liver,[19,20] but the mechanisms have yet to be fully elucidated. Considering the crucial role of ROS in M-MDSC-mediated immunosuppression,[21,22] our integrative analysis indicates that PPP1R15A may serve as a potential regulator in M-MDSCs. Our finding also suggests that PPP1R15A may have a dual biomarker role in both prognosis and ICB response prediction.

To further verify the expression of PPP1R15A in patients with HCC, tumor-adjacent liver and tumor tissues were collected from patients with HCC with liver fibrosis and analyzed by co-immunofluorescence (co-IF) and multi-color flow cytometry. Consistently, we found that the percentages of PPP1R15A$^+$ M-MDSCs in CD45$^+$ leucocytes derived from peripheral blood, tumor, and adjacent liver tissues of patients with HCC were higher than those of healthy donor monocytes (Fig. 2A). Moreover, a higher percentage of PPP1R15A$^+$ M-MDSCs was observed in the livers when compared to blood in patients with HCC (p <0.05; Fig. 2A). In addition, co-IF staining demonstrated strong co-localization of PPP1R15A and MDSC markers CD14 and CD33 in the tumor-surrounding fibrotic livers of patients with HCC (Figs 2B and S1). Using sorted CD45$^+$CD11b$^+$CD33$^+$CD14$^+$HLA-DR$^{-/low}$ M-MDSCs, CD45$^+$CD11b$^+$CD33$^+$CD15$^+$HLA-DR$^{-/low}$ PMN-MDSCs, CD45$^-$ liver cells from patients with fibrosis-associated HCC as well as monocytes from healthy donors for RT-qPCR (reverse transcription-quantitative PCR) analysis, we further confirmed that *PPP1R15A* was significantly upregulated in M-MDSCs (p <0.05; Fig. 2C). Since we have demonstrated that M-MDSCs accumulated in fibrotic livers displayed enhanced immunosuppressive activity compared to their counterparts in blood,[10] these findings suggest the clinical significance of PPP1R15A over-expression and its potential role in M-MDSC-mediated immunosuppression.

PPP1R15A is induced by TGF-β to regulate immunosuppressive activity of M-MDSCs

To investigate the potential functional significance of PPP1R15A in M-MDSCs, we introduced a myeloid cell-competent lentivirus packed with shRNA[17] to knockdown *PPP1R15A* expression in LX2-CM-induced M-MDSCs, followed by phenotypic and immunosuppressive analysis (Fig. 3A). The knockdown efficiency of the lentivirus-shRNA against human *PPP1R15A* (sh*PPP1R15A*) was confirmed by RT-qPCR (p <0.05; Fig. 3B). While the M-MDSC proportion showed a decreasing trend with *PPP1R15A* knockdown (Fig. S2), the expression of immunosuppressive markers (ARG1 and S100A8/9) and ROS production in M-MDSCs were significantly reduced (p <0.05; Fig. 3B,C). More importantly, M-MDSCs with reduced *PPP1R15A* expression exhibited a significantly decreased ability to suppress CD3$^+$ T-cell proliferation (p <0.01; Fig. 3D), demonstrating that PPP1R15A is a key player in M-MDSC-mediated immunosuppression. Accordingly, co-IF demonstrated proximity between PPP1R15A$^+$CD14$^+$ cells and CD8$^+$ T cells in the tumor-surrounding fibrotic livers of patients with HCC (Fig. S3). These results suggest that PPP1R15A$^+$ M-MDSCs may interact closely with CD8$^+$ T cells, potentially via secretion of T-cell chemokines such as CCL3 and CCL4[10,23] (Table S4).

Next, we explored how PPP1R15A is upregulated in HSC-induced M-MDSCs. Transforming growth factor-β (TGF-β) is a key pro-fibrotic factor that is reported to be dramatically elevated in liver fibrosis and to promote M-MDSC differentiation and function.[24,25] Since activated HSCs could produce TGF-β in liver fibrosis,[26] we speculated that activated HSCs may promote M-MDSC generation and immunosuppression through the secretion of TGF-β. To test this hypothesis, we treated healthy donor CD14$^+$ cells with human recombinant TGF-β or LX2-CM-induced M-MDSCs with the TGF-β inhibitor LY2109761 (Fig. 3E). Of note, we found that activation of the TGF-β pathway indicated by Smad2/3 phosphorylation could increase the expression of PPP1R15A in monocytes, leading to the dephosphorylation of eukaryotic translation initiation factor 2 (eIF2α) on serine 51, a direct downstream target of PPP1R15A[27] (Fig. 3F). Complementarily, inhibition of the TGF-β pathway resulted in the reduction of PPP1R15A expression and increase of p-eIF2α in LX2-CM-induced M-MDSCs (Fig. 3G). Since the expression of *PPP1R15A* was also positively correlated with *TGFB1* in tumor-adjacent livers from patients with HCC from the TCGA dataset (n = 48) and liver tissues from the GETx cohort (n = 110) (Fig. S4), our data suggest that TGF-β may be an upstream signal for PPP1R15A induction in M-MDSCs. Moreover, TIDE analysis revealed that the signature scores for TGFB1, MDSCs, and fibrosis (as reflected by cancer-associated fibroblasts) were significantly higher in predicted ICB non-responders compared to responders (Fig. S5), thus supporting their roles in ICB resistance.

Ppp1r15a inhibition suppresses M-MDSC functionality to restrict HCC progression

To further evaluate the effect of PPP1R15A in M-MDSC-mediated immunosuppression and HCC development *in vivo*, we utilized our established fibrosis-associated orthotopic HCC mouse model[15,16] and the myeloid cell-competent

determined by RT-qPCR and Western blot, respectively. GAPDH served as a loading control. (F) TCGA HCC samples with high (n = 109) and low (n = 109) *PPP1R15A* mRNA expression were stratified by top and bottom 30% in 369 patients for the analysis of Kaplan-Meier curves of overall survival (data generated on GEPIA2). (G) Prediction of potential clinical immunotherapy responsiveness in *PPP1R15A*^{high} *vs*. *PPP1R15A*^{low} patients with HCC was shown using the TIDE signature in TCGA HCC samples (p = 0.0001, Chi-square test). DEGs, differentially expressed genes; HCC, hepatocellular carcinoma; HSC, hepatic stellate cell; M-MDSC, monocytic myeloid-derived suppressor cell; scRNA-seq, single-cell RNA-sequencing; TCGA, The Cancer Genome Atlas; TIDE, tumor immune dysfunction and exclusion.

lentivirus packed with shRNA against mouse *Ppp1r15a* (sh*Ppp1r15a*). The knockdown efficiency of lentivirus-sh*Ppp1r15a* was confirmed in bone-marrow-derived M-MDSCs before *in vivo* use[24] (p <0.05; Fig. S6A). Mice fed a HFHC diet for 16 weeks and then treated with lentivirus-sh*Ppp1r15a* or lentivirus expressing shRNA against control (sh*Ctrl*), were then inoculated with RIL-175 tumor cells via intrahepatic injection (Fig. 4A). The development of liver fibrosis and M-MDSC accumulation were confirmed by H&E/Sirius Red staining and flow cytometry analysis (Fig. S6B,C). As expected, selective upregulation of *Ppp1r15a* expression was observed in MDSCs compared to other myeloid cells, T cells, or liver stromal cells in the fibrotic livers (Fig. S6D). We found that lentivirus-sh*Ppp1r15a* effectively downregulated *Ppp1r15a* expression in M-MDSCs sorted from fibrotic livers without influence on mouse body weight (p <0.05; Fig. 4B,C). Of note, knockdown of *Ppp1r15a* in M-MDSCs significantly restricted HCC growth in fibrotic livers (p <0.05; Fig. 4D). Using a spontaneous HCC model induced by STZ injection and HFHC diet,[15] we also showed elevated *Ppp1r15a* expression in fibrosis-associated M-MDSCs that were correlated with tumorigenicity (Fig. S7), thus supporting an important role of Ppp1r15a in fibrosis-associated HCC development.

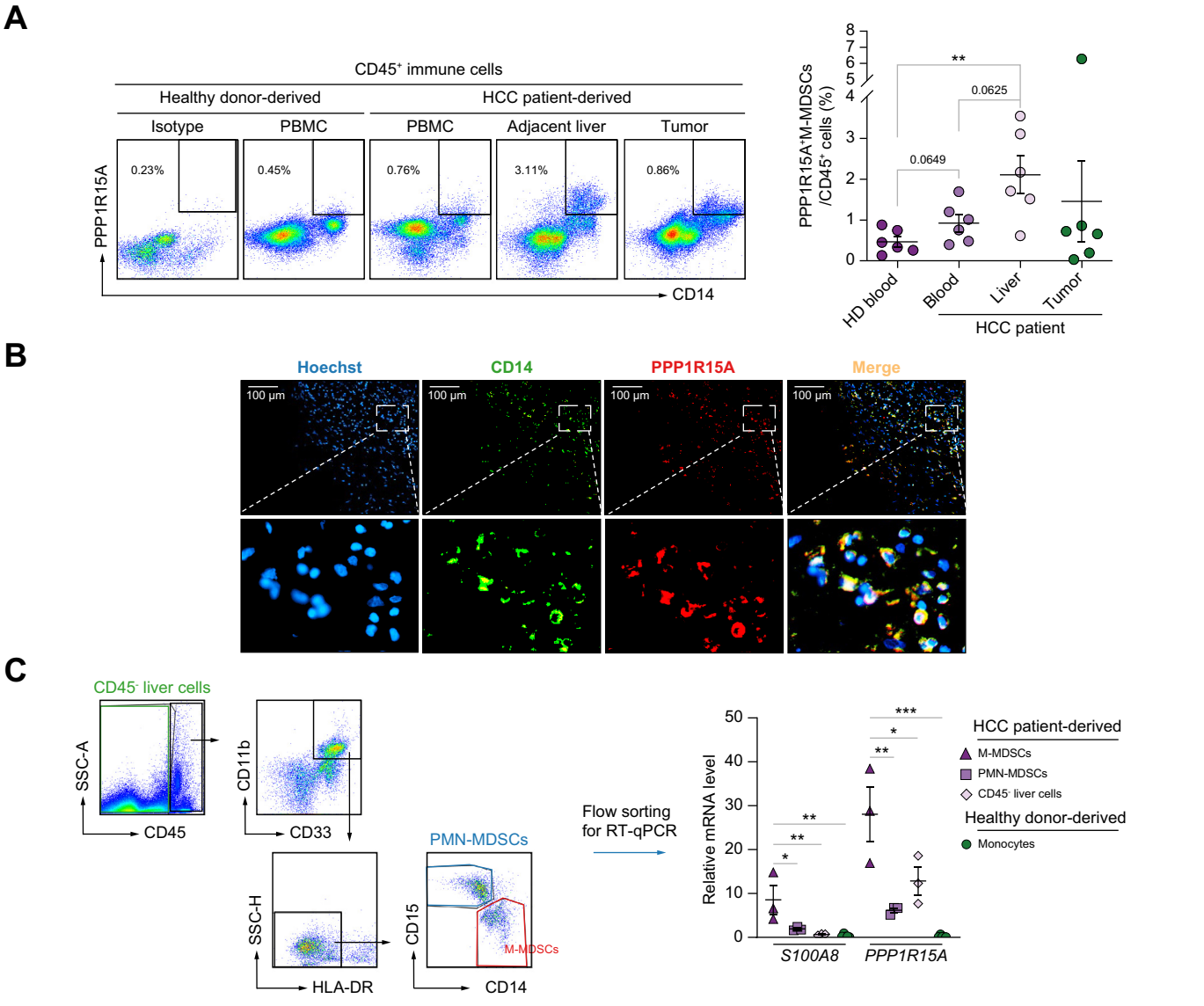

Fig. 2. PPP1R15A is selectively expressed in M-MDSCs from patients with HCC with liver fibrosis. (A) Representative CD14$^+$PPP1R15A$^+$ dot plots and proportions in CD45$^+$ immune cells from healthy donor blood, and blood (*vs*. healthy donor blood, p = 0.0649, Mann-Whitney test), adjacent liver (*vs*. healthy donor blood, p = 0.0087, Mann-Whitney test; *vs*. HCC patient blood, p = 0.0625, Wilcoxon test) and tumor tissues (*vs*. healthy donor blood, p = 0.8182, Mann-Whitney test) from patients with HCC with liver fibrosis (n ≥6). (B) Representative picture of CD14 (green) and PPP1R15A (red) immunofluorescence in the adjacent liver tissues from patients with HCC with liver fibrosis. Co-localization of CD14 and PPP1R15A is shown in the merged image. Hoechst stains for cell nuclei. (n ≥5). (C) *PPP1R15A* (M-MDSC *vs*. PMN-MDSC, p = 0.0015; *vs*. CD45$^-$ liver cells, p = 0.0161; *vs*. monocytes, p = 0.0001) and *S100A8* (M-MDSC *vs*. PMN-MDSC, p = 0.0225; *vs*. CD45$^-$ liver cells, p = 0.0081; *vs*. monocytes, p = 0.0030) mRNA expressions in CD45$^+$CD33$^+$CD11b$^+$CD14$^+$HLA-DR$^{-/low}$ M-MDSCs, CD45$^+$CD33$^+$CD11b$^+$CD15$^+$HLA-DR$^{-/low}$ PMN-MDSCs, and CD45$^-$ liver cells sorted from adjacent livers of patients with HCC with liver fibrosis (n = 3). CD14$^+$ cells sorted from healthy donor PBMCs serve as control. Data were analyzed by one-way ANOVA and presented as mean±SEM. *, p <0.05; **, p <0.01; ***, p <0.001. HCC, hepatocellular carcinoma; M-MDSC, monocytic myeloid-derived suppressor cell; PBMC, peripheral blood mononuclear cell; PMN-MDSC, polymorphonuclear myeloid-derived suppressor cell.

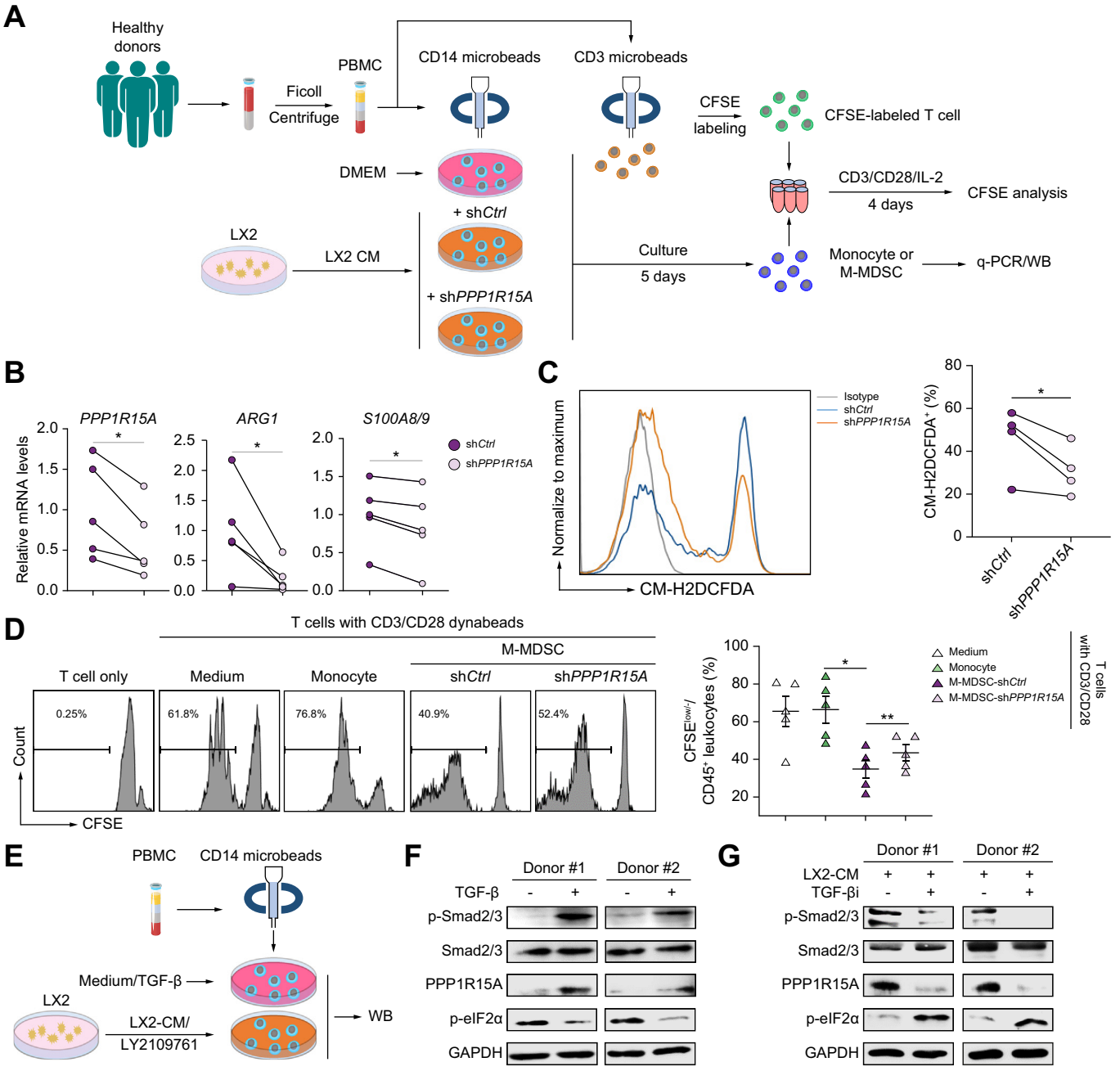

Fig. 3. PPP1R15A is induced by TGF-β to regulate M-MDSC immunosuppression. (A) Schematic diagram of immunosuppression analysis in M-MDSCs under lentivirus-based shRNA treatment *in vitro*. (B) Relative mRNA levels (to *GAPDH*) of *PPP1R15A* (p = 0.0159), *ARG1* (p = 0.03409), *S100A8/9* (p = 0.0104), and (C) representative overlay histogram and percentage of ROS$^+$ cells (p = 0.0466) characterized by DCFDA staining in M-MDSCs treated with lentivirus-sh*Ctrl* or -sh*PPP1R15A* (n≥4). (D) Histogram of CFSE^{low} proliferated CD3$^+$ T cells after co-culture with monocyte, M-MDSC-sh*Ctrl* or -sh*PPP1R15A*. T cells alone with or without simulation by CD3/CD28 Dynabeads served as positive and negative controls, respectively (n = 5) (M-MDSC-sh*Ctrl* *vs*. monocyte, p = 0.0118; *vs*. M-MDSC-sh*PPP1R15A*, p = 0.0035). Data were analyzed by paired t test and presented as mean±SEM. *p <0.05; **p <0.01. (E) Monocytes isolated by CD14 microbeads from healthy donor PBMCs were treated with medium or TGF-β (0.2 ng/ml) or cultured in CM from human-activated HSC line LX2 in the presence of DMSO or TGF-β inhibitor *LY2109761* (4 μM). (F-G) Protein levels of p-smad2/3, smad2/3, PPP1R15A and p-eIF2α in indicated cells were detected by Western blot. GAPDH serves as a loading control. M-MDSC, monocytic myeloid-derived suppressor cell; PBMC, peripheral blood mononuclear cell; ROS, reactive oxygen species; sh, short-hairpin.

We next analyzed the single immune cells isolated from fibrotic livers and tumors of the HFHC diet-induced HCC model mice by multi-color flow cytometry (Fig. S8A). Consistent with our *in vitro* data (Fig. 3B), *Ppp1r15a* knockdown reduced the proportion of immunosuppressive ARG1$^+$S100A9$^+$ M-MDSCs in the liver microenvironment (p <0.05), while increasing the number of IFN-γ$^+$Granzyme B (GZMB)$^+$CD8$^+$ T cells in tumors (p <0.05; Fig. 4E,F). The proportions of hepatic ARG1$^+$S100A9$^+$ M-MDSCs were not only positively correlated with tumor weight (r = 0.7741, p = 0.0004), but also negatively correlated with IFN-γ$^+$GZMB$^+$CD8$^+$ T cells from tumors (r = -0.6803, p = 0.0037; Fig. 4G,H). Moreover,

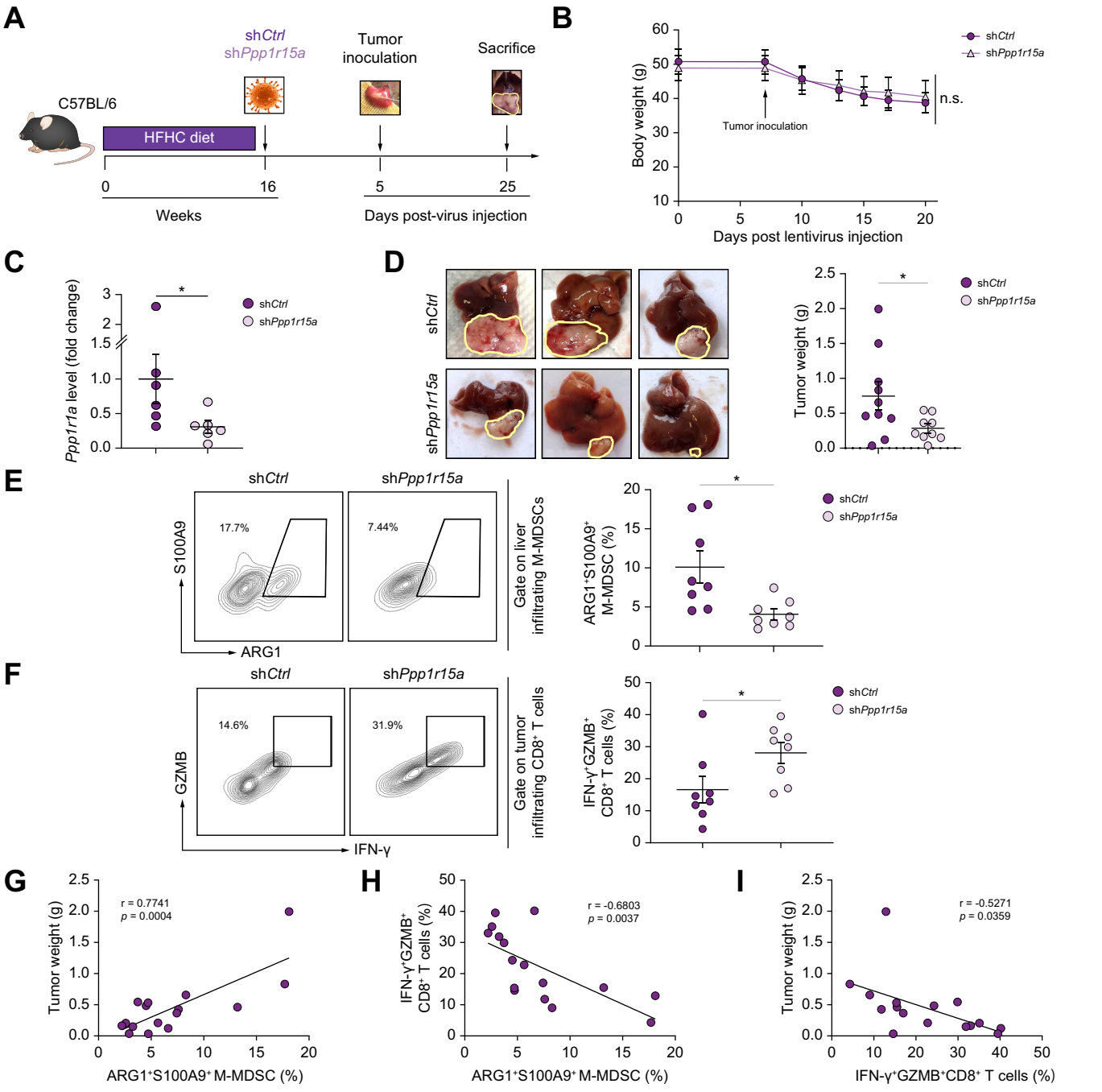

Fig. 4. *Ppp1r15a* inhibition suppresses M-MDSC functionality to restrict HCC progression in the fibrotic liver. (A) Schematic diagram of *Ppp1r15a* knockdown by lentivirus-based shRNA in fibrosis-associated HCC mouse model (n ≥8). (B) Mouse body weights were monitored every other day after lentivirus injection (Two-way ANOVA). (C) Knockdown efficiency of lentivirus-sh*Ppp1r15a* was confirmed by RT-qPCR in M-MDSCs sorted from mouse livers at the endpoint (p = 0.0411, Mann-Whitney test). (D) Representative images of liver and tumor, and tumor weight were shown at the endpoint (p = 0.0431, unpaired t test). (E) Representative flow cytometry density plots and proportions of ARG1$^+$S100A9$^+$ M-MDSCs in liver-infiltrating CD45$^+$ leukocytes (p = 0.0107, unpaired t test) and (F) IFN-γ$^+$GZMB$^+$ cells in CD8$^+$ T cells from tumors were shown (p = 0.0374, unpaired t test). Data were presented as mean±SEM. *p <0.05. (G) Correlations of ARG1$^+$S100A9$^+$ M-MDSC proportions towards tumor weights or (H) IFN-γ$^+$GZMB$^+$CD8$^+$ T cells. (I) Correlation between IFN-γ$^+$GZMB$^+$CD8$^+$ T cells and tumor weight (Pearson correlation). HCC, hepatocellular carcinoma; M-MDSC, monocytic myeloid-derived suppressor cell; RT-qPCR, reverse transcription-quantitative PCR.

IFN-γ$^+$GZMB$^+$CD8$^+$ T cells were associated with tumor suppression, indicating a critical role in anti-tumor function (r = -0.5271, p = 0.0359; Fig. 4I). We also observed an increase of hepatic CD11b$^+$GR-1$^-$F4/80$^+$CD206$^-$ M1 macrophages in the mice receiving lentivirus-sh*Ppp1r15a* injections (p <0.05, Fig. S8B). Since M-MDSCs are reported to show the possibility of differentiating into M1 macrophages,[28] our data implied that PPP1R15A may also function in maintaining M-MDSC status in the tumor-supportive liver microenvironment. Taken together, these data suggest that PPP1R15A is crucial for M-MDSC-mediated immunosuppression and HCC growth in fibrotic liver.

Ppp1r15a inhibition promotes an inflamed TME to enhance ICB efficacy

To further investigate whether targeting *Ppp1r15a* could modulate HCC immunotherapy, we established another fibrosis-related HCC mouse model induced by CCl_4 as previously described[16] (Fig. 5A). Our data showed that lentiviral-mediated *Ppp1r15a* knockdown could improve the anti-tumor efficacy of PD-L1 blockade without affecting the body weight of the treated mice (Fig. 5B,C). Consistent with the HFHC diet-induced fibrosis-related HCC model, *Ppp1r15a* knockdown could efficiently reduce the proportion of $ARG1^+S100A9^+$ M-MDSCs in fibrotic liver, leading to an elevation of tumor-infiltrating IFN-$\gamma^+GZMB^+CD8^+$ T cells when combined with ICB therapy (Fig. 5D,E). Likewise, the proportions of hepatic $ARG1^+S100A9^+$ M-MDSCs were not only positively correlated with tumor weight ($r = 0.6158$, $p = 0.0005$), but also negatively correlated with IFN-$\gamma^+GZMB^+CD8^+$ T cells ($r = -0.3569$, $p = 0.06$; Fig. 5F,G). Moreover, IFN-$\gamma^+GZMB^+CD8^+$ T cells were also correlated with tumor growth inhibition ($r = -0.6147$, $p = 0.0006$; Fig. 5H). Collectively, these findings suggest that *Ppp1r15a* knockdown markedly decreased the number and immunosuppressive activity of M-MDSCs, resulting in an inflamed TME with a high level of cytotoxic $CD8^+$ T cells conducive to anti-tumor immune responses with ICB therapy.

Selective inhibition of PPP1R15A suppresses the identity and immunosuppression in patient-derived M-MDSCs

We next investigated the clinical potential of PPP1R15A inhibition by treating fibrotic HCC patient-derived PBMCs with a specific PPP1R15A inhibitor Sephin1, which can selectively disrupt the formation of the functional PPP1R15A complex.[27] We first tested the dose and efficacy of Sephin1 in HSC-induced M-MDSCs (Fig. 6A). Perturbation of the PPP1R15A pathway by Sephin1 treatment (Fig. 6B) could significantly reduce M-MDSC proportion (p <0.001; Fig. 6C) and ROS production (p <0.001; Fig. 6D), which resulted in impaired M-MDSC-mediated immunosuppression of T-cell proliferation (Fig. 6E). More importantly, treatment of HCC patient-derived PBMCs with Sephin1 (Fig. 6F) also decreased expression of the immunosuppressive marker ARG1 in M-MDSCs (p <0.05; Fig. 6G, while treatment increased the expression of maturation markers CD80 and CD86 (p <0.05; Fig. 6H). In summary, our findings demonstrate the susceptibility of HCC patient-derived M-MDSCs to PPP1R15A inhibition.

PPP1R15A$^+$ M-MDSC signature is associated with poor overall survival and predicted low responsiveness to immunotherapy in patients with cancer

Given the crucial role of M-MDSCs as the Achilles' heel of ICB responsiveness in HCC,[10] we finally evaluated the significance of PPP1R15A on patients' response to ICB therapy. Using the mRNA levels of *PPP1R15A, CD14, ARG1, S100A8, S100A9*, we generated a *PPP1R15A*$^+$ M-MDSC signature for analysis. Firstly, we found that patients with HCC with a high *PPP1R15A*$^+$ M-MDSC signature displayed poor overall survival rates compared to those patients with a low *PPP1R15A*$^+$ M-MDSC signature in the HCC TCGA dataset (p <0.05; Fig. 7A). We next explored the potential associations of the *PPP1R15A*$^+$ M-MDSC signature towards ICB responsiveness in cohorts of patients with HCC,[11] melanoma[29,30] and renal cell carcinoma (RCC).[31] Of note, patients with melanoma receiving an ICB antibody and grouped as responders displayed a lower *PPP1R15A*$^+$ M-MDSC signature compared to those grouped as non-responders in two independent patient cohorts (Fig. 7B). Moreover, a similar pattern was observed in RCC and HCC patient cohorts, in which non-responders displayed a higher *PPP1R15A*$^+$ M-MDSC signature compared to responders (Fig. 7B). Finally, we further grouped patients with high or low baseline *PPP1R15A*$^+$ M-MDSC signatures to analyze the survival benefit of patients under ICB treatment. Consistently, we found that a higher baseline *PPP1R15A*$^+$ M-MDSC signature was associated with worse overall survival of patients with melanoma, RCC and HCC[11,32,33] (Fig. 7C). Taken together, these data implicate the potential predictive role of *PPP1R15A*$^+$ M-MDSCs in ICB responsiveness of patients with cancer.

Discussion

The liver is an immunologic organ that modulates the immune response to cancer arising within it. Accumulating studies have focused on investigating the variable effects of the tumor-surrounding liver microenvironment in modulating tumor immunity, progression, and sensitivity to immunotherapy.[2,34] Since the majority of HCC arises in the context of liver fibrosis,[1] we have established fibrosis-associated HCC models and demonstrated the crucial role of the peritumoral fibrotic liver microenvironment in driving aggressive tumor growth via inducing M-MDSCs through interaction with pro-fibrogenic HSCs.[10] Accordingly, therapeutic approaches that target MDSC expansion, immunosuppression, or recruitment have shown great potential in both preclinical HCC models[8–11] and clinical trials (NCT04123379; NCT02868255; NCT01839604). By integrative analysis of the transcriptomes from liver fibrosis-associated M-MDSCs, we identified PPP1R15A as a critical determinant of M-MDSC-mediated immunosuppression and HCC progression in the fibrotic liver microenvironment. Inhibition of M-MDSC-intrinsic PPP1R15A could restrict tumor growth and potentate ICB responsiveness by releasing M-MDSC-mediated immunosuppression, which in turn potentiated T-cell responses with dramatic production of the cytolytic cytokines IFN-γ and GZMB. Mechanistically, TGF-β induced the upregulation of PPP1R15A in M-MDSCs which in turn triggered the expression of ARG1, S100A8/9, and ROS to potentiate immunosuppression on T cells. Furthermore, PPP1R15A expression was markedly enriched in hepatic M-MDSCs of patients with HCC, in which a *PPP1R15A*$^+$ M-MDSC signature was associated with both poor survival and ICB non-responsiveness. Taken together, we surmise that inhibition of PPP1R15A offers an opportunity for M-MDSC targeting in cancer immunotherapy.

PPP1R15A, also known as GADD34, is a regulatory subunit of protein phosphatase 1 (PP1) that directly targets eIF2α, thus serving a critical role in the regulation of protein translation.[27] The upregulation of PPP1R15A is commonly reported in tumor cells that are associated with cancer progression and poor clinical prognosis in patients with breast cancer, anaplastic thyroid carcinoma, lung carcinoma, colorectal cancer, and HCC.[19,20,35–37] In parallel, tumoral

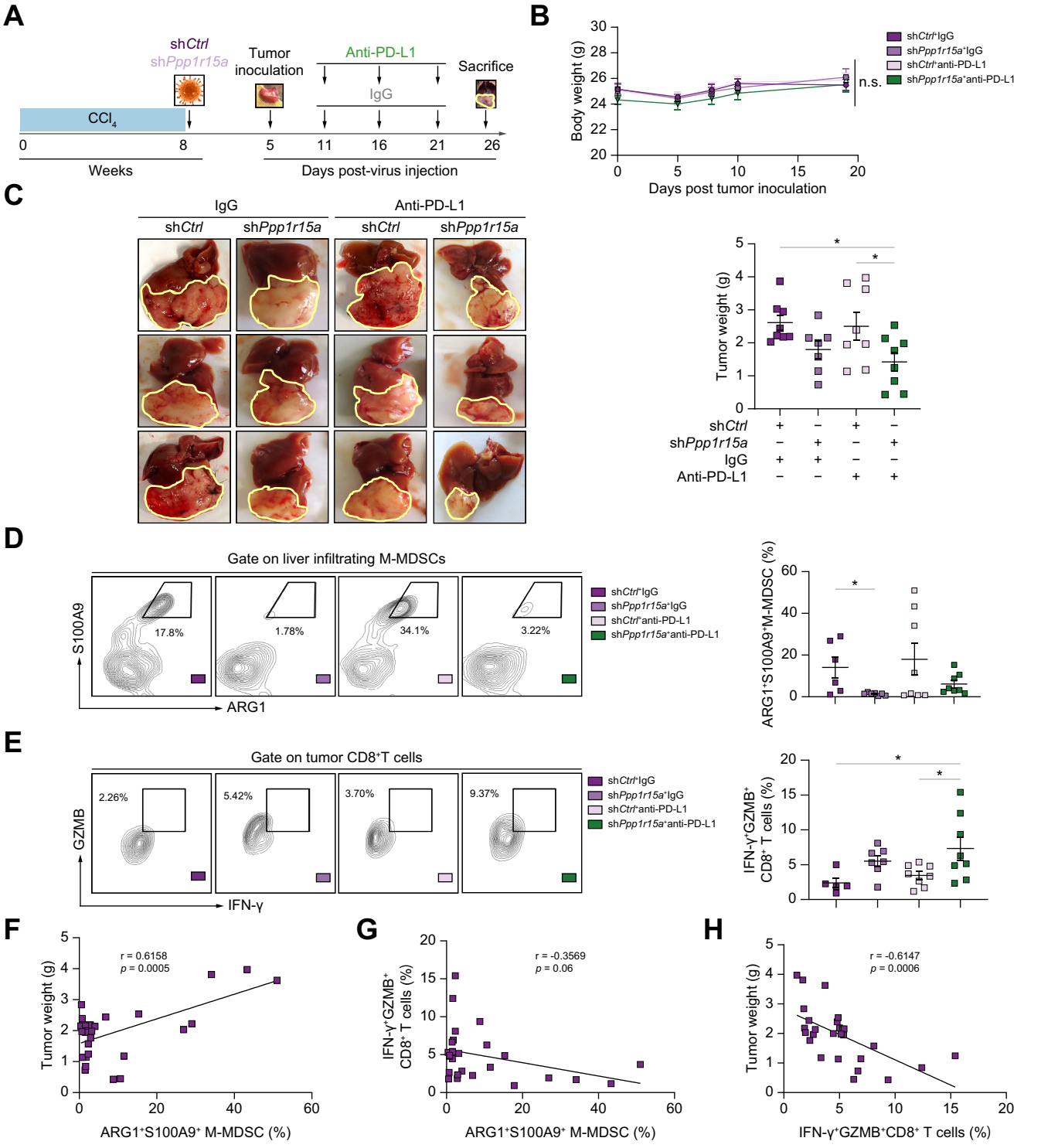

Fig. 5. *Ppp1r15a* inhibition enhances ICB efficacy in HCC. (A) Experimental setting of CCl_4-induced fibrotic HCC in mice. (B) Body weight change (Two-way ANOVA) and (C) tumor weight of control, single treatment, or combination therapy in CCl_4-induced HCC (combo *vs*. control, $p = 0.0251$; *vs*. anti-PD-L1, $p = 0.0448$). (D) The proportions of hepatic ARG1$^+$S100A9$^+$ M-MDSCs ($p = 0.0396$) and (E) intratumoral IFN-γ$^+$GZMB$^+$CD8$^+$ T cells in different groups (combo *vs*. control, $p = 0.0179$; *vs*. anti-PD-L1, $p = 0.0360$). Data were analyzed by one-way ANOVA and shown as mean±SEM. *p <0.05. (F-G) Correlations of hepatic ARG1$^+$S100A9$^+$ M-MDSCs towards tumor weight or intratumoral IFN-γ$^+$GZMB$^+$CD8$^+$ T cells. (H) Correlation between IFN-γ$^+$GZMB$^+$CD8$^+$ T cells and tumor weight in CCl_4-induced HCC (Pearson correlation). CCl_4, carbon tetrachloride; HCC, hepatocellular carcinoma; ICB, immune checkpoint blockade; M-MDSC, monocytic myeloid-derived suppressor cell.

PPP1R15A knockdown has been reported to sensitize HCC cells to sorafenib *in vitro* and in xenograft models.[36] Using a diethylnitrosamine-induced HCC mouse model, Chen *et al.* showed that the increased expression of PPP1R15A in tumor cells induced by DNA damage and endoplasmic reticulum stress promotes hepatic damage and inflammation to

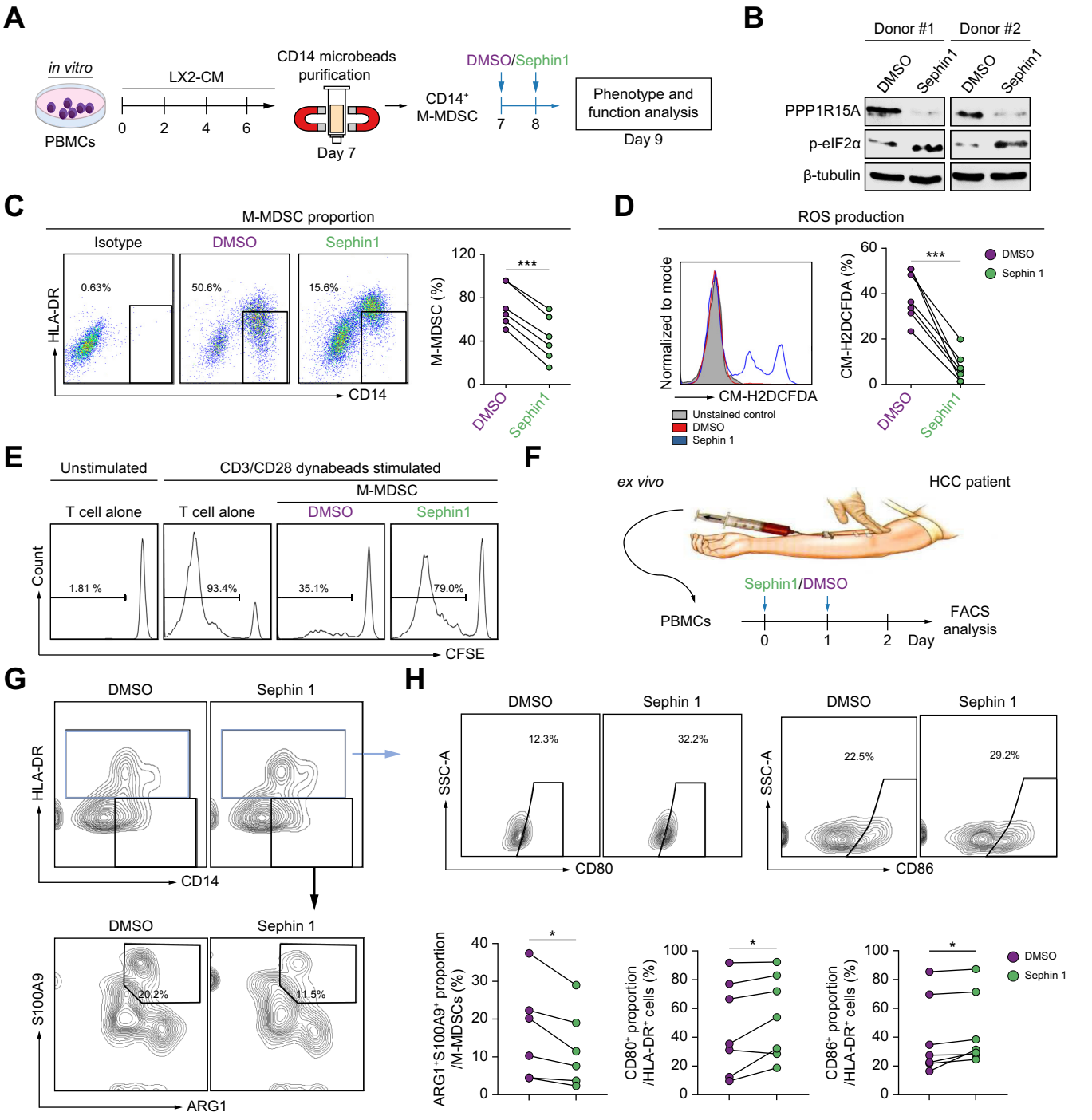

Fig. 6. Selective inhibition of PPP1R15A suppresses M-MDSC identity and immunosuppression. (A) Schematic diagram of Sephin1 (5 μM) treatment regimen in LX2-CM-induced M-MDSCs. (B) Western blot analysis for the expressions of PPP1R15A, p-eIF2α in LX2-CM-induced M-MDSCs treated with DMSO or Sephin1. β-tubulin served as a control. (C) Representative flow cytometry dot plots and proportions of M-MDSCs with or without Sephin1 treatment (n = 6) (p <0.0001, paired t test). (D) Representative overlay histogram and percentage of ROS$^+$ cells characterized by CM-H2DCFDA staining in CD14$^+$ cells with or without Sephin1 treatment (n = 4) (p = 0.0002, paired t test). (E) Histogram of CFSE^{low} proliferated CD3$^+$ T cells after co-culture with MDSCs upon DMSO or Sephin1 treatment. T cells alone with or without simulation by CD3/CD28 Dynabeads served as positive and negative controls, respectively. (F) Schematic diagram of Sephin1 (5 μM) treatment regimen in fibrosis-associated HCC patient-derived PBMCs. (G) Representative flow cytometry density plots of ARG1$^+$S100A9$^+$ populations in CD45$^+$CD11b$^+$CD33$^+$CD14$^+$HLA-DR$^{-/low}$ M-MDSCs (p = 0.0257, paired t test) as well as (H) CD80$^+$ (p = 0.0469, Wilcoxon test) and CD86$^+$ (p = 0.0156, Wilcoxon test) populations in HLA-DR$^+$ cells from HCC patient-derived PBMCs with or without Sephin1 treatment (n ≥6). Data were presented as mean±SEM. *p <0.05; ***p <0.001. CM, conditioned medium; HCC, hepatocellular carcinoma; M-MDSC, monocytic myeloid-derived suppressor cell; PBMC, peripheral blood mononuclear cell.

advance hepatocarcinogenesis.[20] Since the tumor nodules are remarkably reduced in the whole-body *Ppp1r15a* knockout mice, this report provides solid evidence that PPP1R15A enhances HCC development.[20] In addition to the tumor cell-intrinsic effect, our findings further pinpointed that PPP1R15A is also highly expressed in M-MDSCs in the

tumor-supportive liver microenvironment. Suppression of PPP1R15A in M-MDSCs not only decreases their immunosuppressive ability but also restricts HCC growth in fibrotic liver. Therefore, given both the tumor- and M-MDSC-intrinsic effects, our data highlighted the multiple facets of PPP1R15A in promoting tumor immunosuppression and hepatic carcinogenesis, suggesting that PPP1R15A is an exploitable druggable target for HCC therapy.

We and others have interrogated the crosstalk between HSCs and MDSCs in promoting cancer progression, metastasis, and immunotherapy resistance.[10,38,39] The activated HSC has been established as a central driver of liver fibrosis that also contributes to liver immune tolerance through interaction with monocytes.[38,39] Mechanistically, the activated HSCs could polarize monocytes to immunosuppressive M-MDSCs via physical interaction by CD44-CD44L, or

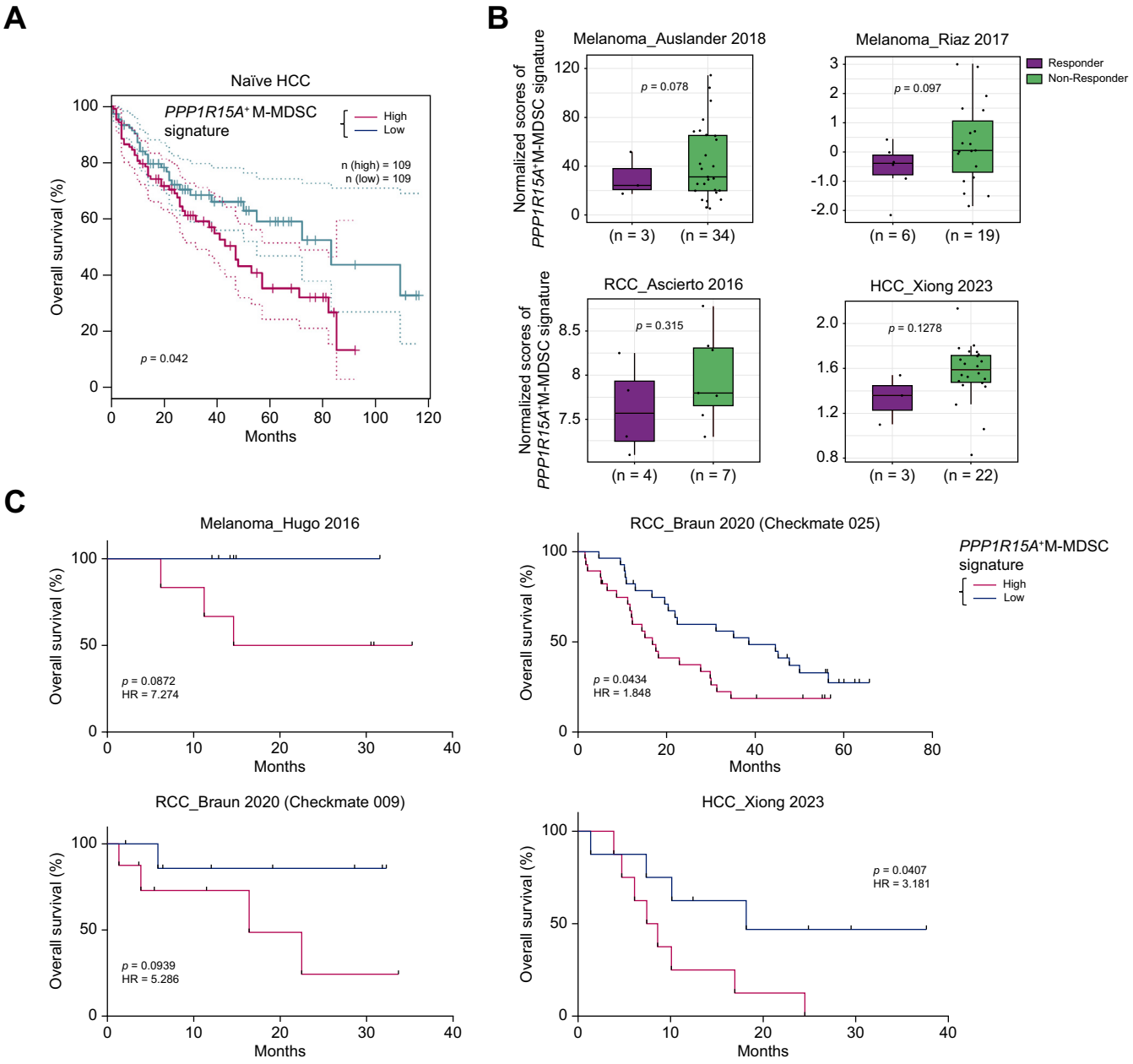

Fig. 7. *PPP1R15A*$^+$ M-MDSC signature is associated with poor overall survival and immunotherapy unresponsiveness in patients with cancer. (A) TCGA HCC samples with high (n = 109) and low (n = 109) *PPP1R15A*$^+$ M-MDSC signatures (indicated by mRNA levels of *PPP1R15A, CD14, ARG1, S100A8, S100A9*) were stratified by top and bottom 30% in 369 patients (data generated on GEPIA). Kaplan-Meier curves of overall survival in patients with HCC according to the levels of *PPP1R15A*$^+$ M-MDSC signatures. (B) *PPP1R15A*$^+$ M-MDSC signature in patients' grouped as responders (including complete response and partial response and non-responders (including stable disease or progressive disease) according to RECIST v1.1 among patients with melanoma, ccRCC and HCC treated by ICB. Data were analyzed by unpaired t test and presented as mean±SD. (C) Kaplan-Meier survival analyses of ICB-treated patients with melanoma, ccRCC and HCC according to their baseline *PPP1R15A*$^+$ M-MDSC signature (Log-rank test). ccRCC, clear cell renal cell carcinoma; HCC, hepatocellular carcinoma; ICB, immune checkpoint blockade; M-MDSC, monocytic myeloid-derived suppressor cell; TCGA, The Cancer Genome Atlas.

soluble factors including cyclooxygenase-2, IL-6, TNF-α and TGF-β.[38,39] We have observed a gradual increase and significant accumulation of PPP1R15A expression upon LX2-CM stimulation. Among different soluble factors in LX2-CM, we further identified TGF-β as the main driver of PPP1R15A upregulation in M-MDSCs. Of note, apart from HSCs, TGF-β can also be derived from other cells such as tumor cells. Interestingly, Liu *et al.* pointed out that tumoral PPP1R15A expression could promote the secretion of VEGF A and TGF-β in Lewis lung carcinoma mouse model,[37] suggesting that the TGF-β/PPP1R15A axis may function as a self-reinforcing signaling. In addition, PPP1R15A is reported to be required for optimal transcription and production of the cytokines IFN-β and IL-6 as well as iNOS.[40] Our data further showed that PPP1R15A functioned in promoting M-MDSC immunosuppression by upregulating the expression of immunosuppressive molecules such as ARG1 and S100A8/9 as well as ROS production. Taken together, these data suggested that PPP1R15A may promote cancer progression by inducing the expression of pro-inflammatory cytokines and immunosuppressive factors from both tumor cells and M-MDSCs.

One of the limitations of the current study is the orthotopic mouse model using a hepatoma cell line. We are aware that insights from the orthotopic HCC mouse model may not fully recapitulate the heterogenous immune features of patients and have provided limited predictions for outcomes in the clinic. In parallel, the molecular basis of modulation of ARG1/S100A/ROS production by PPP1R15A in M-MDSCs is also unknown. Nevertheless, our data suggest that specific inhibition of PPP1R15A could reduce M-MDSC development and immunosuppression, which in turn could break the immunosuppressive barrier to restrict tumor progression and enhance the efficacy of immunotherapies in HCC and potentially other M-MDSC-enriched cancers. Further investigations on dosage optimization and efficacy testing of selective PPP1R15A inhibition[27] in combination with ICB should provide proof-of-concept for preclinical studies and future human translation.

Affiliations

[1]*School of Biomedical Sciences, The Chinese University of Hong Kong, Hong Kong, China;* [2]*Chongqing Key Laboratory for the Mechanism and Intervention of Cancer Metastasis, Chongqing University Cancer Hospital, Chongqing, China;* [3]*Department of Gastroenterology, The First Affiliated Hospital, Sun Yat-Sen University, Guangzhou, China;* [4]*Department of Liver Surgery, Ren Ji Hospital, School of Medicine, Shanghai Jiao Tong University, Shanghai, China;* [5]*Department of Clinical Oncology, Sir YK Pao Centre for Cancer, The Chinese University of Hong Kong, Hong Kong, China;* [6]*Department of Anatomical and Cellular Pathology, The Chinese University of Hong Kong, Hong Kong, China;* [7]*Department of Surgery, The Chinese University of Hong Kong, Hong Kong, China;* [8]*State Key Laboratory of Translational Oncology, The Chinese University of Hong Kong, Hong Kong, China;* [9]*Lee Kong Chian School of Medicine, Nanyang Technological University, Singapore;* [10]*State Key Laboratory of Digestive Disease, The Chinese University of Hong Kong, Hong Kong, China*

Abbreviations

ARG1, arginase-1; CFSE, carboxyfluorescein succinimidyl ester; CM, conditioned medium; DEGs, differentially expressed genes; eIF2α, eukaryotic translation initiation factor 2; GADD34, growth arrest and DNA damage-inducible protein 34; GZMB, Granzyme B; HCC, hepatocellular carcinoma; HFHC, high-fat-high-carbohydrate; HSC, hepatic stellate cell; ICB, immune checkpoint blockade; IFN, interferon; LIHC, liver hepatocellular carcinoma; MDSC, myeloid-derived suppressor cell; M-MDSC, monocytic myeloid-derived suppressor cell; NSCLC, non-small cell lung cancer; PBMC, peripheral blood mononuclear cell; PD-L1, programmed cell death ligand 1; PMN-MDSC, polymorphonuclear myeloid-derived suppressor cell; PP1, protein phosphatase 1; PPP1R15A, protein phosphatase 1 regulatory subunit 15A; RCC, renal cell carcinoma; ROS, reactive oxygen species; S100A8/9, S100 calcium binding protein A8/A9; scRNA-seq, single-cell RNA-sequencing; shRNA, short-hairpin; TCGA, The Cancer Genome Atlas; TGF-β, transforming growth factor-β; TIDE, tumor immune dysfunction and exclusion; TME, tumor microenvironment; VEGF, vascular endothelial growth factor.

Financial support

This project is supported by the University Grants Committee through General Research Fund (14108219, 14115820, 14120621, 14107622), the Health and Medical Research Fund (07180556), the Li Ka Shing Foundation, the CUHK Strategic Seed Funding for Collaborative Research Scheme, and the support (funding and study medications) by Merck Sharp and Dohme (MSD-IIS 55253). Xiaoyu Liu is supported by the Fundamental Research Funds for the Central Universities (2023CDJYGRH-YB03) and the Project for Enhancing Scientific Research Capabilities of Chongqing University Cancer Hospital (2023nlts007).

Conflict of interest

The authors of this study declare that they do not have any conflict of interest.

Please refer to the accompanying ICMJE disclosure forms for further details.

Authors' contributions

Study concept and design: X.L, J.Z, and A.S.L.C. Data acquisition and analysis: X.L, M.L, W.T, W.Y, L.Z, S.C, Z.X, J.L, W.W.Y.S.T, T.S, J.L, C.Z, T.T.K, and J.Z. Bioinformatics analysis: H.W, T.T.H.C, and J.C; Clinical resources: H.S, H.H.W.L, J.W, P.B.S.L, K.F.T, and S.L.C. Writing of manuscript: X.L, J.Z, and A.S.L.C. Supervision: T.X, J.Z, and A.S.L.C; Funding acquisition: X.L, J.J.Y.S, S.L.C, J.Z, and A.S.L.C.

Data availability statement

The data that support the findings in this study are included in the manuscript and/or its supplementary materials.

Acknowledgments

We thank Prof. Tim F. Greten (National Cancer Institute, National Institutes of Health, Bethesda, USA) and Prof. Lars Zender (University Hospital Tubingen, Germany) for providing us with the RIL175 cell line. We thank Prof. Nathaniel R. Landau (New York University School of Medicine) for providing us with the backbone plasmids used for lentivirus construction.

Supplementary data

Supplementary data to this article can be found online at https://doi.org/10.1016/j.jhepr.2024.101087.

References

Author names in bold designate shared co-first authorship

[1] El-Serag HB. CURRENT CONCEPTS hepatocellular carcinoma. New Engl J Med 2011;365(12):1118–1127.

[2] Llovet JM, Castet F, Heikenwalder M, et al. Immunotherapies for hepatocellular carcinoma. Nat Rev Clin Oncol 2022;19(3):151–172.

[3] **Foerster F**, **Gairing SJ**, Ilyas SI, et al. Emerging immunotherapy for HCC: a guide for hepatologists. Hepatology 2022;75(6):1604–1626.

[4] Ding L, Wang N, Wang Q, et al. Midkine inhibition enhances anti-PD-1 immunotherapy in sorafenib-treated hepatocellular carcinoma via preventing immunosuppressive MDSCs infiltration. Cell Death Discov 2023;9(1):92.

[5] Finn RS, Qin SK, Ikeda M, et al. Atezolizumab plus bevacizumab in unresectable hepatocellular carcinoma. New Engl J Med 2020;382(20):1894–1905.

[6] Zhu AX, Abbas AR, de Galarreta MR, et al. Molecular correlates of clinical response and resistance to atezolizumab in combination with bevacizumab in advanced hepatocellular carcinoma. Nat Med 2022;28(8):1599–1611.

[7] Tcyganov EN, Hanabuchi S, Hashimoto A, et al. Distinct mechanisms govern populations of myeloid-derived suppressor cells in chronic viral infection and cancer. J Clin Invest 2021;131(16).

[8] Zhou J, Liu M, Sun H, et al. Hepatoma-intrinsic CCRK inhibition diminishes myeloid-derived suppressor cell immunosuppression and enhances immune-checkpoint blockade efficacy. Gut 2018;67(5):931–944.

[9] **Sun H**, **Yang W**, **Tian Y**, et al. An inflammatory-CCRK circuitry drives mTORC1-dependent metabolic and immunosuppressive reprogramming in obesity-associated hepatocellular carcinoma. Nat Commun 2018;9(1):5214.
[10] **Liu M**, **Zhou JY**, Liu XY, et al. Targeting monocyte-intrinsic enhancer reprogramming improves immunotherapy efficacy in hepatocellular carcinoma. Gut 2020;69(2):365–379.
[11] **Xiong Z**, **Chan SL**, **Zhou J**, et al. Targeting PPAR-gamma counteracts tumour adaptation to immune-checkpoint blockade in hepatocellular carcinoma. Gut 2023;72(9):1758–1773.
[12] **Bronte G**, **Petracci E**, **De Matteis S**, et al. High levels of circulating monocytic myeloid-derived Suppressive-like cells are associated with the primary resistance to immune checkpoint inhibitors in advanced non-small cell lung cancer: an Exploratory analysis. Front Immunol 2022;13:866561.
[13] Sade-Feldman M, Kanterman J, Klieger Y, et al. Clinical significance of circulating CD33+CD11b+HLA-DR- myeloid cells in patients with stage IV melanoma treated with ipilimumab. Clin Cancer Res 2016;22(23):5661–5672.
[14] Sharma A, Seow JJW, Dutertre CA, et al. Onco-fetal reprogramming of endothelial cells drives immunosuppressive macrophages in hepatocellular carcinoma. Cell 2020;183(2):377–394. e21.
[15] Tang W, Zhou J, Yang W, et al. Aberrant cholesterol metabolic signaling impairs antitumor immunosurveillance through natural killer T cell dysfunction in obese liver. Cell Mol Immunol 2022;19(7):834–847.
[16] Liu X, Zhou J, Wu H, et al. Fibrotic immune microenvironment remodeling mediates superior anti-tumor efficacy of a nano-PD-L1 trap in hepatocellular carcinoma. Mol Ther 2023;31(1):119–133.
[17] **Bobadilla S**, **Sunseri N**, Landau NR. Efficient transduction of myeloid cells by an HIV-1-derived lentiviral vector that packages the Vpx accessory protein. Gene Ther 2013;20(5):514–520.
[18] **Jiang P**, **Gu S**, **Pan D**, et al. Signatures of T cell dysfunction and exclusion predict cancer immunotherapy response. Nat Med 2018;24(10):1550–1558.
[19] Tanaka Y, Ito S, Oshino R, et al. Effects of growth arrest and DNA damage-inducible protein 34 (GADD34) on inflammation-induced colon cancer in mice. Br J Cancer 2015;113(4):669–679.
[20] Chen N, Nishio N, Ito S, et al. Growth arrest and DNA damage-inducible protein (GADD34) enhanced liver inflammation and tumorigenesis in a diethylnitrosamine (DEN)-treated murine model. Cancer Immunol Immunother 2015;64(6):777–789.
[21] Corzo CA, Cotter MJ, Cheng P, et al. Mechanism regulating reactive oxygen species in tumor-induced myeloid-derived suppressor cells. J Immunol 2009;182(9):5693–5701.
[22] Condamine T, Kumar V, Ramachandran IR, et al. ER stress regulates myeloid-derived suppressor cell fate through TRAIL-R-mediated apoptosis. J Clin Invest 2014;124(6):2626–2639.
[23] **Galeano Nino JL**, **Pageon SV**, **Tay SS**, et al. Cytotoxic T cells swarm by homotypic chemokine signalling. Elife 2020;9.
[24] **Lee CR**, **Lee W**, Cho SK, et al. Characterization of multiple cytokine combinations and TGF-beta on differentiation and functions of myeloid-derived suppressor cells. Int J Mol Sci 2018;19(3).
[25] **Cao P**, **Sun ZJ**, **Zhang FL**, et al. TGF-Beta enhances immunosuppression of myeloid-derived suppressor cells to induce transplant immune tolerance through affecting arg-1 expression. Front Immunol 2022;13.
[26] Dewidar B, Meyer C, Dooley S, et al. TGF-Beta in hepatic stellate cell activation and liver fibrogenesis-updated 2019. Cells 2019;8(11).
[27] Das I, Krzyzosiak A, Schneider K, et al. Preventing proteostasis diseases by selective inhibition of a phosphatase regulatory subunit. Science 2015;348(6231):239–242.
[28] **Tcyganov E**, **Mastio J**, Chen E, et al. Plasticity of myeloid-derived suppressor cells in cancer. Curr Opin Immunol 2018;51:76–82.
[29] Auslander N, Zhang G, Lee JS, et al. Robust prediction of response to immune checkpoint blockade therapy in metastatic melanoma. Nat Med 2018;24(10):1545–1549.
[30] **Riaz N**, **Havel JJ**, **Makarov V**, et al. Tumor and microenvironment evolution during immunotherapy with nivolumab. Cell 2017;171(4):934–949 e16.
[31] Ascierto ML, McMiller TL, Berger AE, et al. The intratumoral balance between metabolic and immunologic gene expression is associated with anti-PD-1 response in patients with renal cell carcinoma. Cancer Immunol Res 2016;4(9):726–733.
[32] **Hugo W**, **Zaretsky JM**, Sun L, et al. Genomic and transcriptomic features of response to anti-PD-1 therapy in metastatic melanoma. Cell 2016;165(1):35–44.
[33] Braun DA, Hou Y, Bakouny Z, et al. Interplay of somatic alterations and immune infiltration modulates response to PD-1 blockade in advanced clear cell renal cell carcinoma. Nat Med 2020;26(6):909–918.
[34] Kubes P, Jenne C. Immune responses in the liver. Annu Rev Immunol 2018;36(36):247–277.
[35] **Cao X**, **Dang L**, **Zheng X**, et al. Targeting super-enhancer-driven oncogenic transcription by CDK7 inhibition in anaplastic thyroid carcinoma. Thyroid 2019;29(6):809–823.
[36] **Gan G**, **Shi Z**, **Shangguan C**, et al. The kynurenine derivative 3-HAA sensitizes hepatocellular carcinoma to sorafenib by upregulating phosphatases. Theranostics 2021;11(12):6006–6018.
[37] Liu LT, Ito S, Nishio N, et al. GADD34 promotes tumor growth by inducing myeloid-derived suppressor cells. Anticancer Res 2016;36(9):4623–4628.
[38] **Xu Y**, **Zhao W**, Xu J, et al. Activated hepatic stellate cells promote liver cancer by induction of myeloid-derived suppressor cells through cyclooxygenase-2. Oncotarget 2016;7(8):8866–8878.
[39] **Hochst B**, **Schildberg FA**, Sauerborn P, et al. Activated human hepatic stellate cells induce myeloid derived suppressor cells from peripheral blood monocytes in a CD44-dependent fashion. J Hepatol 2013;59(3):528–535.
[40] **Clavarino G**, **Claudio N**, Dalet A, et al. Protein phosphatase 1 subunit Ppp1r15a/GADD34 regulates cytokine production in polyinosinic:polycytidylic acid-stimulated dendritic cells. Proc Natl Acad Sci U S A 2012;109(8):3006–3011.

Keywords: M-MDSCs; immunosuppression; PPP1R15A; liver fibrosis; HCC.
Received 24 April 2023; received in revised form 24 March 2024; accepted 27 March 2024; Available online 4 April 2024